TISSUE ENGINEERING
Volume 12, Number 4, 2006

Analysis of Cell Growth in Three-Dimensional Scaffolds

JAMES C.Y. DUNN, M.D., Ph.D.,[1,2] WAN-YIN CHAN,[1] VITTORIO CRISTINI, PH.D.,[4] J.S. KIM, Ph.D.,[5] JOHN LOWENGRUB, Ph.D.,[5] SHIVANI SINGH,[1] and BENJAMIN M. WU, D.D.S., Ph.D.[1,3]

ABSTRACT

The *in vitro* growth of pre-osteoblasts in multi-layer, three-dimensional scaffolds was determined from experimental measurements and was compared to a mathematical model. Immediately following cell seeding, the initial cell density was uniform throughout the scaffold. After 10 days, the cell density increased from 2.1×10^5 cells/cm^3 to 1.3×10^7 cells/cm^3 at the fluid-scaffold interface. The increase in cell density was largely confined to the outermost 200 μm from the fluid-scaffold interface. The cell density profile was in good agreement with a mathematical model that simulated the cell growth based on the local oxygen tension. The improved understanding derived from this mathematical model may be useful in the design of three-dimensional scaffolds that can support more uniform growth of cells.

INTRODUCTION

A COMMON APPROACH IN TISSUE ENGINEERING is to fabricate three-dimensional precursor tissue analogs from cells, scaffolds, and signaling molecules.[1] A critical design criterion for such tissue-engineering constructs is to support the growth of cells within the scaffold so that the precursor analog may transform into the tissue of interest. For very thin tissues such as the skin,[2] standard techniques are often sufficient for the *in vitro* cultivation of cells grown on two-dimensional surfaces. In contrast, even for thin, porous, three-dimensional scaffolds, heterogeneous growth can result, with a confluent layer of cells at the outer surface of the scaffold and limited, non-uniform growth in the inner core.[3–5] For thicker tissues such as bone and liver, standard cell culture techniques do not work well in three-dimensional scaffolds. As the thickness of the precursor tissue analog and the cell density increase within the scaffold, the limitation of solute transport becomes apparent. This effect of scaffold thickness has been observed in many three-dimensional tissue-engineering systems, where the growth of cells is restricted to a few hundred microns from the fluid-tissue interface.[6–8] This length scale is similar to the characteristic length for solute diffusion in tissues, where the average inter-capillary distance is on the order of a hundred microns, depending on the metabolic activity of the particular tissue.[9,10] Compared to the *in vivo* tissues with rich capillary networks, the *in vitro* precursor tissue analogs lack vascularization to support the solute transport within the interior of the scaffolds. Cells located in the interior of the scaffold rely on diffusion for solute transport and are compromised by the depletion of nutrients by cells located near the outer surface.

A variety of techniques have been employed to overcome the transport limitation *in vitro,* including the use of perfusion in bioreactors so that convection minimizes the diffusion constraints within the scaffold.[11–13] Vun-

[1]Department of Bioengineering, [2]Department of Surgery, [3]Department of Materials Science & Engineering, University of California, Los Angeles, California.
[4]Department of Biomedical Engineering, [5]Department of Mathematics, University of California, Irvine, California.

jak-Novakovic *et al.* used spinner flasks to seed 2-5 mm thick, 5–10 mm diameter scaffolds and reported good cell distribution, but an outer surface zone with 60–70% higher cell density still persisted.[14] Similar findings are reported with spinner flask seeding of 13 mm diameter × 3 mm thick polyglycolide mesh scaffolds.[15] Although such convective approaches address the *in vitro* transport problem, the ability to provide equivalent convective transport *in vivo* is limited. The time lag between nutrient depletion within the implanted scaffold and nutrient replenishment from angiogenesis is often the limiting factor against uniform cell-growth within large scaffolds.[16] The small penetration depth may be due to limited seeding, inadequate nutrient delivery to meet the metabolic demands of the cells, or inadequate waste elimination.[17,18] Collectively, the literature suggests that engineering of thick tissues is limited by nutrient transport and that initial homogenous cell distribution is not sufficient to produce final uniform distribution.

To quantify the role of initial spatial distribution on the transport process in tissue-engineering systems, a mathematical model was developed to simulate the cell growth as a function of the environmental parameters. The model takes into account the influence of the cell growth on the temporal and spatial variation of a proliferation-limiting critical molecule, such as oxygen, as well as the reciprocating influence of the distribution of the critical molecule on cell growth. The predicted growth rates were compared against experimentally measured cell growth in multi-layer, three-dimensional scaffolds with controlled spatial distribution of cells.

MATERIALS AND METHODS

Scaffold fabrication

Polymeric scaffolds were made by the solvent casting/particulate leaching technique. A 15% (w/w) polymer solution was prepared by dissolving 2.7 g of 85:15 polylactide co-glycolide (PLGA; intrinsic viscosity ~0.6; Absorbable Polymers International, Pelham, AL) in 15.3 g of chloroform (Sigma, St. Louis, MO). Subsequently, 0.5 g of the 15% polymer solution was mixed with 1.48 g of sucrose (pre-sieved 200–300 μm; C&H Sugar, Costco, Los Angeles, CA) and 0.22 g of methanol (Sigma). The mixture was packed into Teflon molds (internal diameter 10 mm, height 1 mm) and was allowed to dry for 4 h inside the molds. Each scaffold was then de-molded and was allowed to dry overnight. The next day, the dried scaffolds were transferred to mesh holders and were subjected to solvent removal by supercritical carbon dioxide fluid extraction for 2 h at 35°C and 870 PSI (Model SFE 500, Thar Technologies, Pittsburgh, PA). Scaffolds were leached in deionized water under ultraviolet light for at least 18 h before cell seeding.

Cell culture

After leaching, each scaffold was immersed in 100 μg/mL of fibronectin (Sigma) in phosphate-buffered saline (PBS) for 5 h. The scaffolds were then transferred to 48-well plates and rinsed with PBS twice. MC3T3-E1 pre-osteoblasts (ATCC, Manassas, VA) were counted using a hemocytometer to determine the approximate cell concentration. Each scaffold was seeded with 1×10^5 MC3T3 cells in 100 μL of α-minimum essential medium (Invitrogen, Carlsbad, CA) by pipetting the cell suspension directly on top of each scaffold. The seeded scaffolds were placed in the incubator (37°C, 5% CO_2) for 4 h to allow for cell adherence. Scaffolds used for the 4 h study were processed immediately for histology while the remaining scaffolds were replenished with 500 μL of complete media (α-medium, 10% FBS, 50 μg/mL L-ascorbic acid and 10 mM beta-glycerol phosphate). The day after cell seeding, the medium was aspirated and the scaffolds were rinsed twice with PBS. Scaffolds were stacked in two patterns shown in Figure 1. Construct A contained five, stacked scaffolds, alternating between cell-seeded and unseeded. Construct B contained five scaffolds all seeded with cells. Each scaffold was 10 mm in diameter and 1 mm in height, making the final height of the constructs 5 mm. To prevent constructs from separating in solution, each construct was weighed down with a square Teflon mesh piece. Complete media (2 mL) was added to each well. All constructs were incubated at 37°C in 5% CO_2, and the medium was changed every 2 days. After 10 days of incubation, the middle scaffold (the third slice) from constructs A and B was fixed and embedded for image analysis.

Scaffold processing for histology

The selected scaffolds were placed in 48-well plates for two rinses of PBS and fixed with 10% formalin and 25% sucrose in PBS for 24 h. The scaffolds were immersed in 4 mL of embedding media consisting of 5% type A porcine skin gelatin and 5% sucrose in deionized water at 40°C for 2 h to allow infusion of the embedding media throughout the scaffold.[19] After the scaffolds were frozen in a dry ice-acetone bath, they were stored at −80°C until cryosectioning. Sequential sections (10 μm thick) were obtained, starting from the bottom of each scaffold. The first section that contained any part of the scaffold was considered the bottom of the scaffold, and subsequent sections were taken at 50, 150, 250, 350, 450, 550, 650, 750, 850, and 950 μm until the top of the scaffold was reached. Each section was transferred to a glass slide. Each 10 μm cryosection was stained by DAPI mounting medium (Vector Laboratories, Burlingame, CA) to visualize the nuclei. The microscopic structure of the highly porous scaffold cultured with pre-osteoblasts was reported previously.[19]

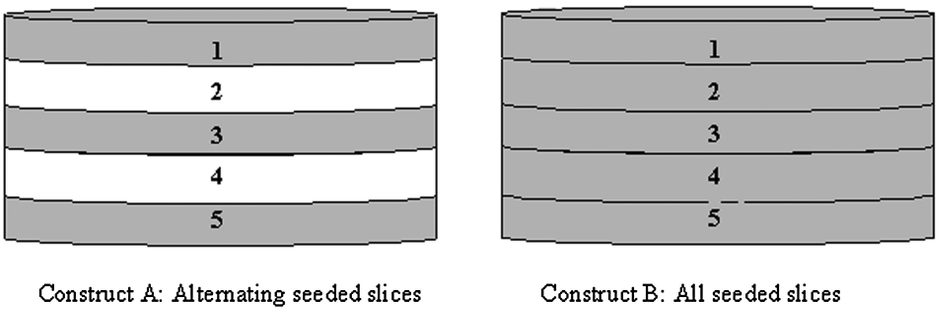

FIG. 1. Stacking patterns for constructs A (alternating seeding) and b (uniform seeding).

Image analysis

Images of each cryosection were captured by a RGB color digital camera (Optronics, Goleta, CA) at 100 × on a Leica DM IRB light microscope (Leica Microsystems, Bannockburn, IL) equipped with motorized x-y stages for automated image acquisition. The number of cells and cell distribution on each section was determined by counting DAPI-labeled cells under fluorescence using the Bioquant Nova software (Bioquant Image Analysis, Nashville, TN). Each section was made up of an average of 96 fields of views. The x and y coordinates of each cell were also recorded and cell number within every 100 μm interval was calculated along two orthogonal orientations (from top to bottom and from left to right) using the x and y coordinate information. The center of each section was set to be the origin. Based on this setting, each counted cell was assigned Cartesian coordinates, and the distance of each cell to the center was determined as $(x^2 + y^2)^{0.5}$. The cell density was determined by counting the number of cells within successive 200 μm thick annulus from the edge to the center of the scaffold.

Model development

It is hypothesized that a limiting molecule, likely oxygen, diffuses across the fluid-scaffold interface and is consumed by cells located near the interface. The scaffold is assumed to be stable over the time course of the experiment. The total rate of consumption of this limiting molecule is proportional to the local cell density, and the specific rate of uptake by the cells is assumed to be proportional to the local concentration of the molecule. The mass balance for this system is governed by the continuity equation.

$$\frac{\partial C}{\partial t} = \nabla \cdot D\nabla C - VCU \tag{1}$$

C: concentration of the critical molecule [mole/mL]
D: diffusivity of critical molecule [cm^2/s]
V: kinetic constant for the specific consumption rate of the critical molecule [mL/s/cell]
U: cell density in the tissue [cell/mL]

The growth of cells in tissue culture can be modeled using the logistic law. During the growth phase, the rate of cell growth is proportional to the cell density modified by the logistic law until the maximal cell density is reached. The specific rate of cell growth is assumed proportional to the concentration of the limiting molecule:

$$\frac{\partial U}{\partial t} = \lambda CU\left(1 - \frac{U}{U_m}\right) \tag{2}$$

λ: kinetic constant for the specific rate of cell growth [mL/mole/s]
U_m: maximal cell density [cell/mL]

The governing equations can be made non-dimensional by introducing dimensionless variables $C' = C/C_0$, where C_0 represents the concentration of the limiting molecule in the bulk fluid, $U' = U/U_m$, $x' = x/L$, and $t' = t/T$. The length scale L is defined to be the characteristic diffusion length:

$$L \equiv \sqrt{\frac{D}{VU_m}}, \tag{3}$$

where the diffusivity D is assumed constant. The time scale T is taken to be the characteristic time for cell growth, *i.e.,*

$$T = 1/(\lambda C_0). \tag{4}$$

This gives the following non-dimensional system:

$$\frac{\partial U'}{\partial t'} = C'U'(1 - U'), \tag{5}$$

for cell-growth, and for the limiting molecule,

$$\frac{T_D}{T}\frac{\partial C'}{\partial t'} = \nabla' \cdot \nabla' C' - C'U', \tag{6}$$

where $T_D = L^2/D$ is the characteristic time scale for diffusion.

In typical tissue culture systems, the approximate value of oxygen diffusivity (D) is 2×10^{-5} cm^2/s, the dissolved oxygen concentration (C_0) is 10^2 nmole/mL, the specific oxygen consumption is 10^{-6} nmole/s/cell so that V is estimated to be 10^{-8} mL/s/cell, and the maximal cell density (U_m) is 10^7 cells/mL[6]. These values yield a characteristic length scale L of 140 μm, which is on the order of the length scale that has been observed experimentally.

In typical cells, the growth rate λC_0 is 1 day^{-1}. Thus, the characteristic time for cell growth, $T = 1/(\lambda C_0) \sim 1$ day, is much longer than the characteristic time for diffusion, $T_D = L^2/\mathrm{D} \sim 10$ s. Since, the ratio $T_D/T << 1$, a quasi-steady approximation of equation (6) is used and the time derivative is dropped. This yields the governing equations:

$$0 = \nabla'^2 C' - C'U'$$
$$\frac{\partial U'}{\partial t'} = C'U'(1 - U') \tag{7}$$

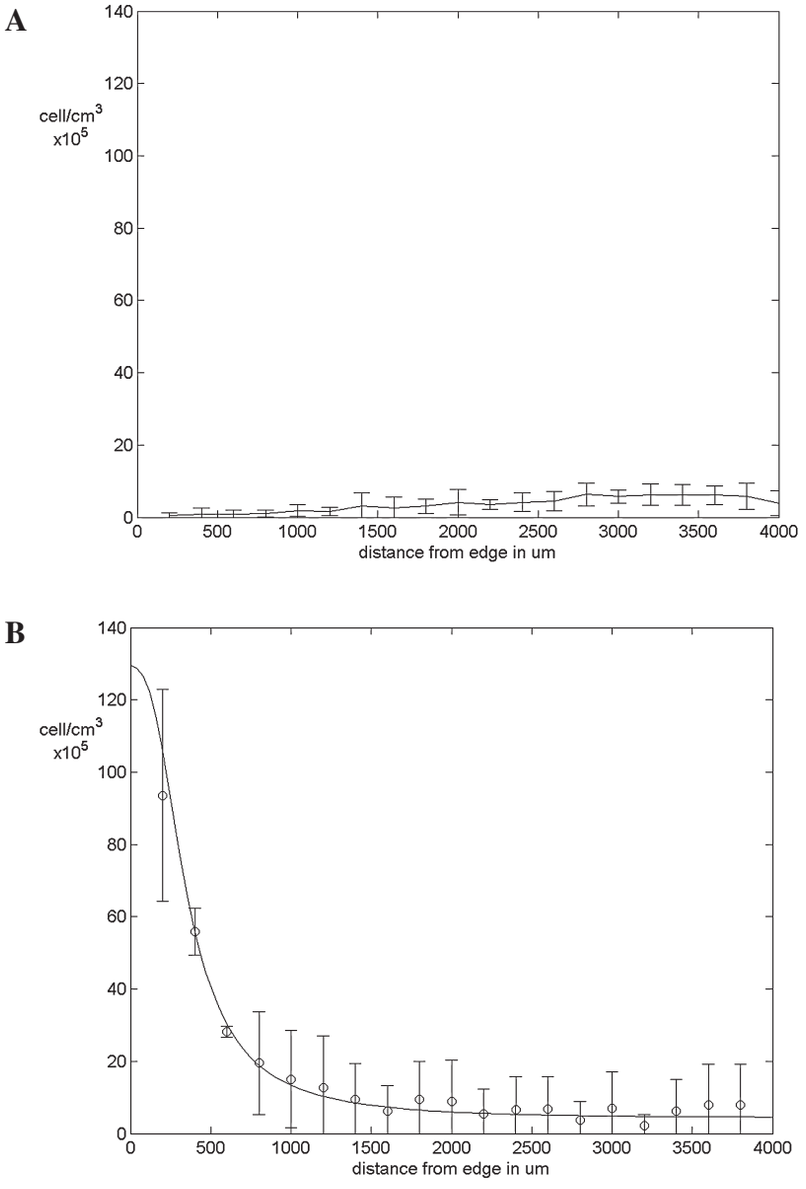

FIG. 2. **(A)** Measured cell density 4 h after seeding scaffolds. **(B)** Measured and simulated cell density for the third scaffold in construct B on day 10. Error bar represents the standard deviation of the measured cell density. Solid line represents numerical simulation with $L = 167$ μm.

The initial conditions are

$$C'(x',0) = 1$$
$$U'(x',0) = U_0/U_m$$

where U_0 is the initial cell density. The boundary condition is

$$C'(x'_\Sigma) = 1$$

where x'_Σ denotes a point on the fluid-scaffold interface. This assumes the limiting molecule concentration is constant in the fluid region in the exterior of the scaffold.

Numerical method

The system of partial differential equations (7) in the axisymmetric (r-z) geometry is solved using a second-order accurate finite difference scheme for the concentration coupled with a second-order accurate Runge-Kutta time discretization scheme for cell density. The algorithm for the concentration field is a simplified version of that developed by Kim *et al.* in the context of phase transitions.[20] The singularity at the origin $r = 0$ in the discrete

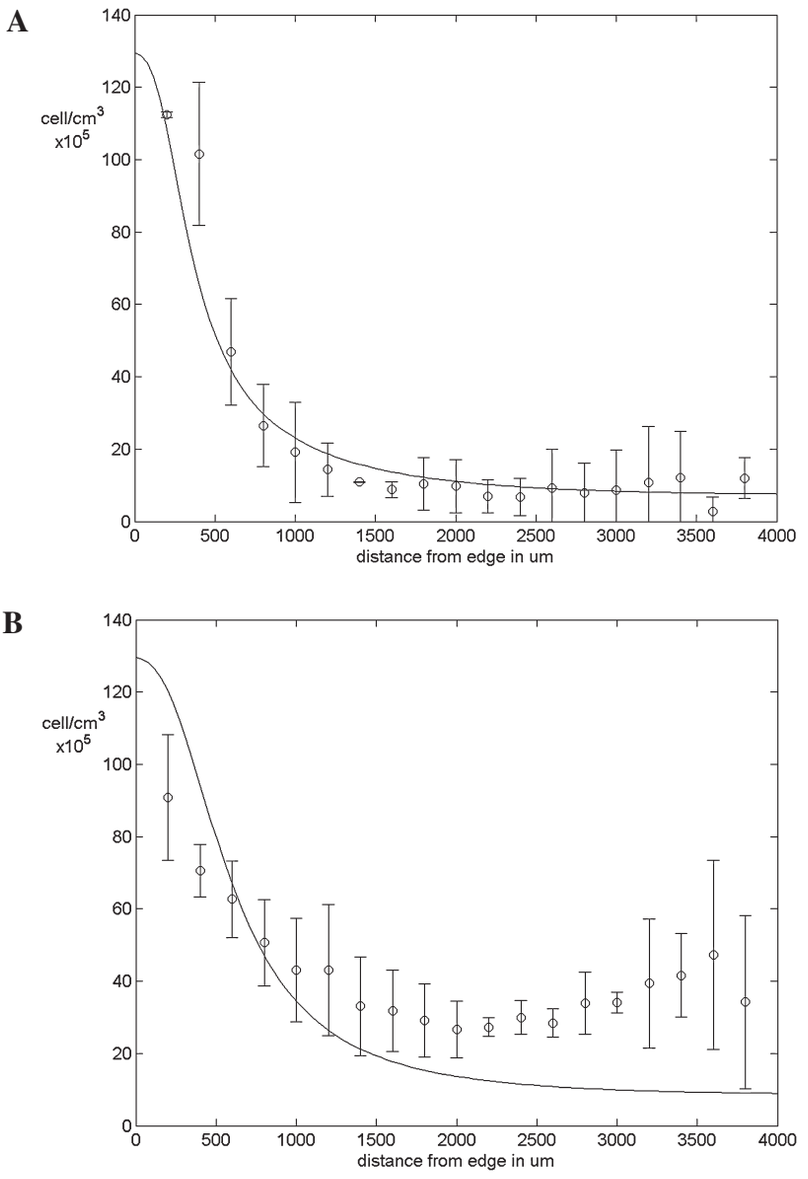

FIG. 3. Measured and simulated cell density for the third scaffold in construct A on day 10. **(A)** Middle portions. **(B)** Top and bottom portions. Error bar represents the standard deviation of measured cell density. Solid line represents numerical simulation with $L = 167$ μm.

axisymmetric concentration equation is avoided using a staggered mesh where the nutrient concentrations and cell densities are determined at grid-cell centers. The corresponding discrete linear system is solved efficiently using a multi-grid method.[21]

RESULTS

Initial cell seeding

The initial cell density and distribution were determined from sections taken after 4 h of seeding and culture. This allowed sufficient time for the initial cell attachment to withstand the subsequent fixing and embedding procedures, but insufficient time for significant cell proliferation. Cell position was determined at various depths throughout the scaffold. Cells were distributed evenly throughout the scaffold (Fig. 2A), indicating a highly interconnected scaffold with sufficient pore size to allow cells to settle evenly. An average of 170 cells was counted per a 10 μm section, yielding an average initial density of 2.1×10^5 cells/cm^3 in the scaffold.

Cell growth in scaffolds

After 10 days of culture, the cell density markedly increased along the outer shell of the cylindrical scaffolds for both constructs A and B, reaching a maximal cell density of 1.3×10^7 cells/cm^3. For construct B, where all scaffolds were uniformly seeded with cells, the cell density decreased rapidly toward the center the scaffold, reaching 10^6 cells/cm^3 at a distance beyond 1 mm from the edge of the scaffold (Fig. 2B). This cell density profile was similar to sections taken from the middle portion of the third scaffold in construct A, where scaffolds were alternately seeded with cells (Fig. 3A). For sections taken from the top or bottom portion of the third scaffold in construct A, the cell density profile also decreased toward the center of the scaffold but reached a higher density, 3×10^6 cells/cm^3, at a distance beyond 1 mm from the edge (Fig. 3B).

Numerical simulations

The system of equations (7) is solved using $U_0/U_m = 0.016$, the ratio of initial cell density to maximal cell density, for constructs A and B. The calculation is volume-averaged in 100×200 μm^2 bins around the middle of the scaffold. The bins partition the scaffold in the radial direction, ranging from the center to the edge of the scaffold. The contours of the numerical simulated cell density for constructs A and B on day 10 are shown in Figure 4. The maximal cell density of 1.3×10^7 cells/cm^3 is achieved along the fluid-scaffold interface for both constructs. The cell density in the top and bottom portions of the third scaffold is slightly higher than that in the middle portion of the third scaffold in construct A (Fig. 4A). This reflects the additional source of oxygen from the adjacent, unseeded scaffolds in construct A. An inner core with cell density $<10^6$ cells/cm^3 occurs beyond 3 mm from the fluid-scaffold interface in the third scaffold in construct A. In contrast, for construct B the

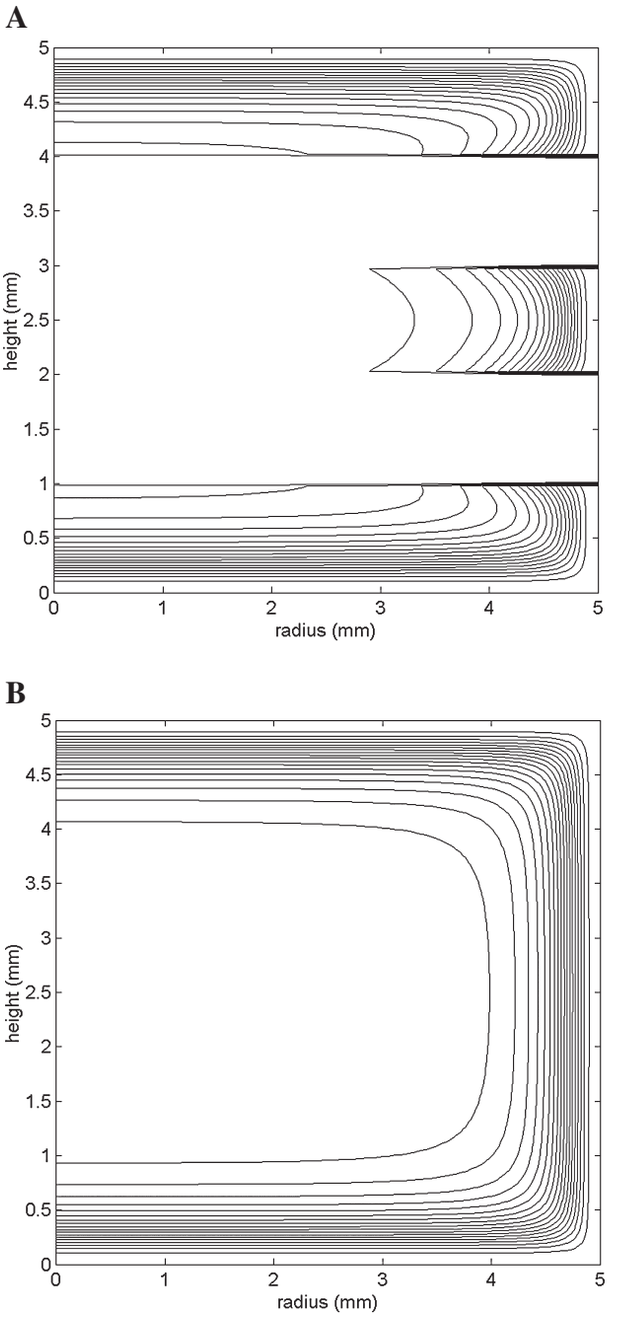

FIG. 4. Numerical simulation of the cell density for the stacked scaffolds in construct A **(A)** and construct B **(B)** on day 10 with $L = 167$ μm. Contours increase by 6.5×10^5 cells/cm^3 from 1.3×10^6 cells/cm^3 to 1.3×10^7 cells/cm^3 at the fluid-scaffold boundary. The third scaffold is represented in the region between 2 mm and 3 mm in height.

cell density contours are concentrated along the fluid-scaffold interface in the third scaffold, leaving a larger core with cell density $<10^6$ cells/cm^3, which occurs beyond 1 mm from the fluid-scaffold interface (Fig. 4B). The contours of the numerically simulated oxygen concentration are plotted for constructs A and B at day 10 (Fig. 5). In construct B, the oxygen concentration drops below 5 nmole/mL, equivalent to 1% oxygen, at a distance of 1 mm from the fluid-scaffold interface in the third scaffold (Fig. 5B). This is due to the high rates of oxygen consumption by the high density of cells at the boundary. This results in a large core of severely hypoxic cells in construct B. In construct A, the unseeded scaffolds facilitate contour extension into the scaffold interior, resulting in a smaller core of severely hypoxic cells, starting at 3 mm from the fluid-scaffold interface in the third scaffold (Fig. 5A).

Good agreement was found between the numerical simulations and the measured cell density for the third scaffold in construct B (Fig. 2B). For the third scaffold in construct A, the simulation was also in reasonable agreement with the measured cell density in the middle portion of the scaffold (Fig. 3A). In the top and bottom portions of the scaffold, near the scaffold layer–scaffold layer interface, the simulation predicted significantly lower cell density as compared to the measurement near the center of the third scaffold in construct A (Fig. 3B).

Two parameters, the time scale T and the length scale L, control the numerical simulation. The length scale L reflects the balance of the oxygen diffusion and oxygen consumption, and the time scale T is a function of the growth rate. The sensitivities of the numerical simulations to these model parameters were examined by varying the values of T and L. For construct B, the numerical simulation predicted a higher cell density away from the edge as L was increased from 100 to 333 μm (Fig. 6). The best fit to the experimental data was when $L = 167$ μm. Using this length scale, as the time scale T was increased from 5 to 40 days, the predicted cell density continued to increase, mostly within the first 1000 μm (Fig.6). For construct A, the numerical simulation also predicted a higher cell density away from the edge as L was increased from 100 to 500 μm (Fig. 7). For the middle portion of construct A, the best data fit was when L = 250 μm. For the top and bottom portions of construct A, when L was 500 μm, the predicted cell density matched the experimental data near the center of the scaffold, but the overall fit of the data was still poor. Using the length scale of 167 μm, as the time scale T was increased from 5 to 40 days, the cell density increased as expected (Fig. 8).

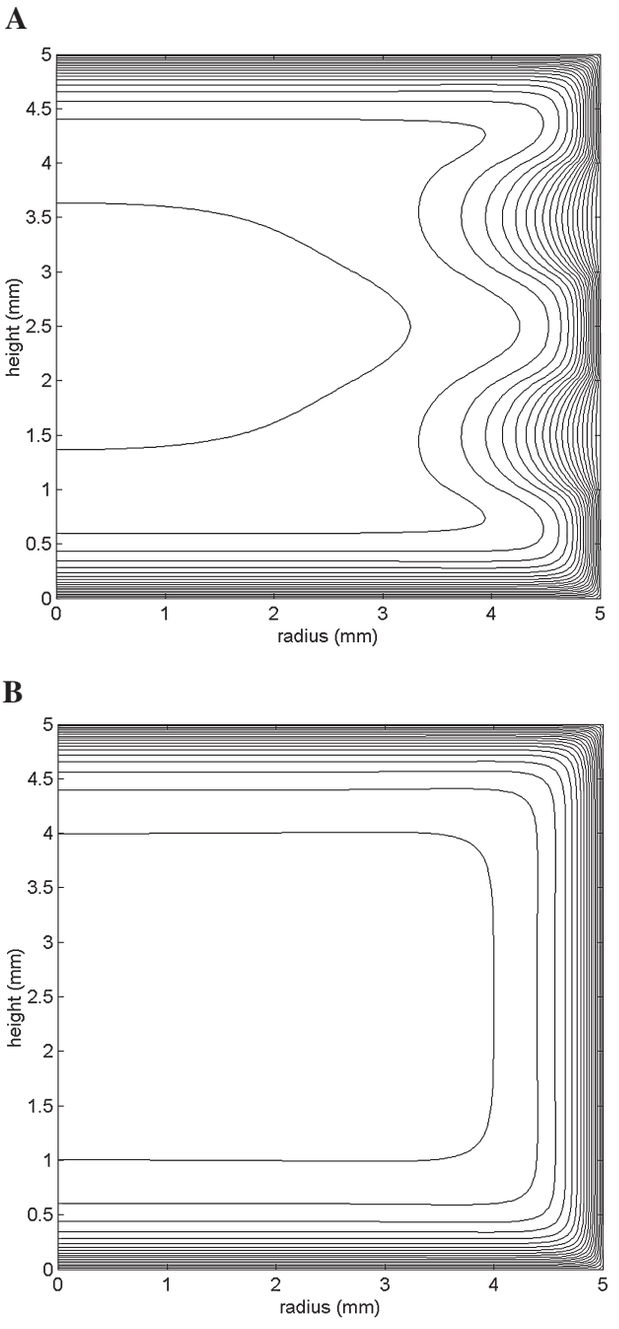

FIG. 5. Numerical simulation of the oxygen concentration for the stacked scaffolds in construct A **(A)** and construct B **(B)** on day 10 with $L = 167$ μm. Contours increase by 5 nmole/mL from 5 nmole/mL to 100 nmole/mL at the fluid-scaffold boundary. The third scaffold is represented in the region between 2 mm and 3 mm in height.

DISCUSSION

Consistent with the existing literature, the growth of pre-osteoblasts in three-dimensional scaffolds was limited to a few hundred microns from the fluid-scaffold interface. It is speculated that this growth pattern was largely governed by the diffusion of oxygen, and a model was developed to simulate the oxygen concentration within the scaffold and to predict the cell growth based

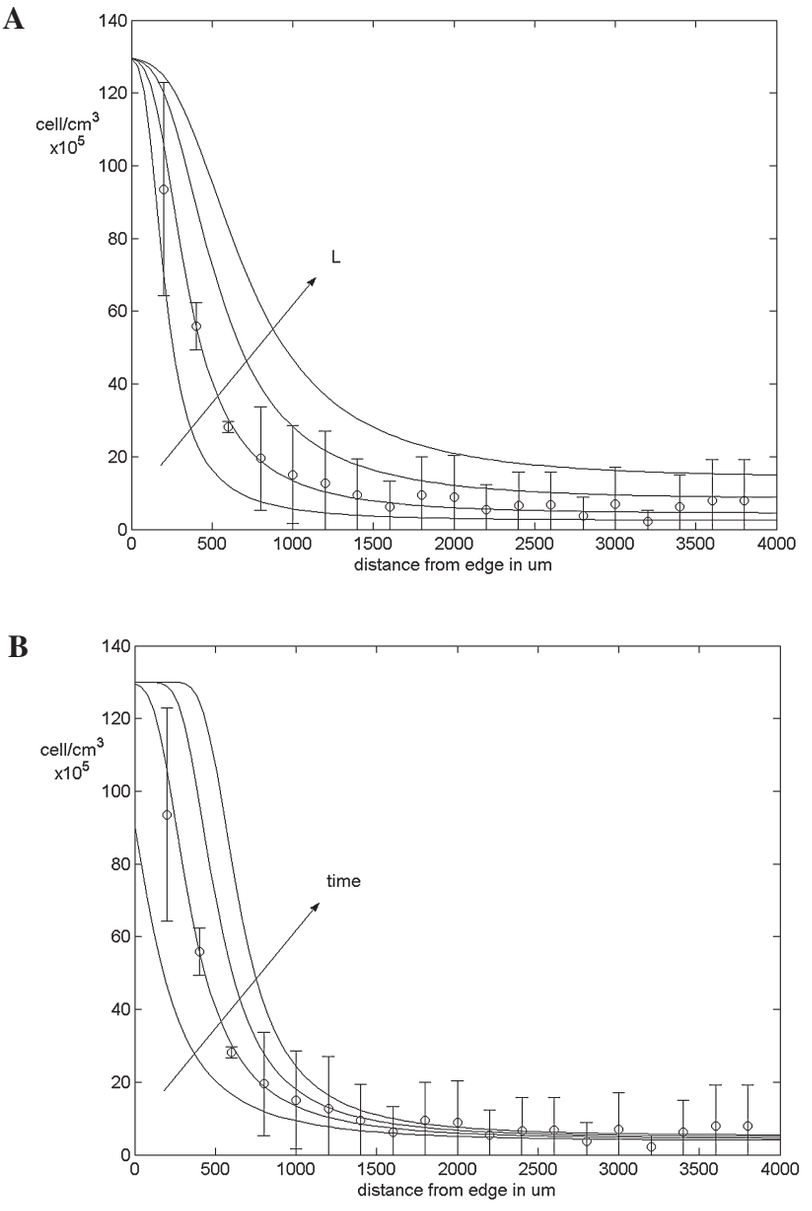

FIG. 6. Effect of varying the characteristic length and time on simulated cell density for the third scaffold in construct B. **(A)** Length scales $L = 100$, 167, 250, and 333 μm on day 10. **(B)** Length scale $L = 167$ μm on day 5, 10, 20, and 40.

on the local oxygen concentration. Good agreement was found between experimental data and mathematical simulations, except in the boundary between the cell-seeded scaffold and the non-seeded scaffold where the model predicted less cell growth.

In the analysis of the model, two important parameters controlled the cell distribution within the scaffold: the length scale L, which is the characteristic length scale for diffusion, and the time scale T, which is the reciprocal of the specific cell growth rate. The length scale represents the characteristic distance within which the cells have adequate oxygen to grow. By comparing the experimental data to the simulation results, the length scale that most closely matched the data was found to be between 100 and 200 μm. This length scale is similar to the normal physiologic environment where the average inter-capillary distance is a few hundred microns. The calculated value of 140 μm for L using literature values for oxygen diffusivity and consumption is also within this range. This suggests that the proposed model can be used to predict the cell growth for a variety of cell types and scaffold configurations, based solely on the oxygen diffusivity, the oxygen consumption, and the oxygen-dependent growth rate.

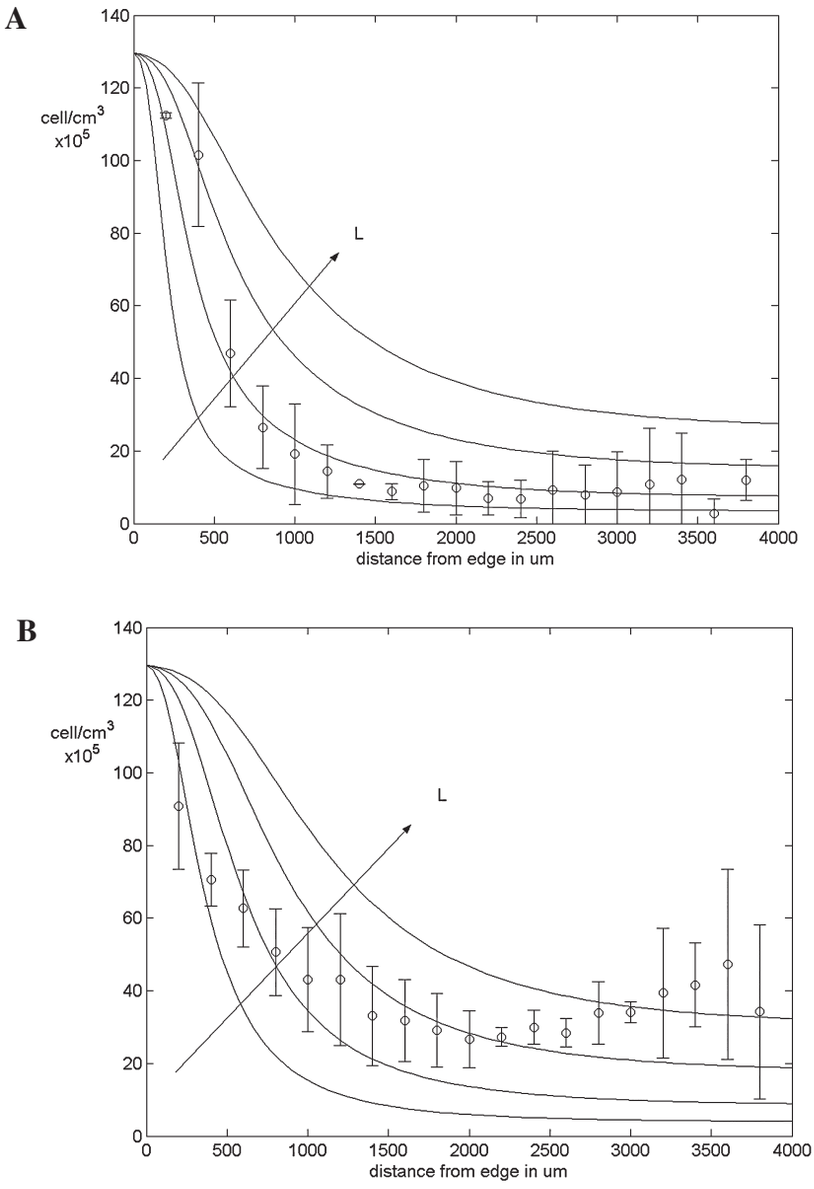

FIG. 7. Effect of varying the characteristic length on simulated cell density for the third scaffold in construct A on day 10. The simulated cell density for the middle portion **(A)** and the top and bottom portions **(B)** with length scales $L = 100$, 167, 250, and 333 μm.

In the present model, first-order kinetics was employed for oxygen consumption, which was similar to that used by others in the literature.[17,18] Previous models employed a volume-averaging approach to simplify the two-phase system for cells growing on scaffolds.[17,18] In these models, the oxygen consumption was first-order but did not depend on local cell density. The difference in the present model was the inclusion of the local cell density in the reaction term so that the rate of oxygen consumption was proportional to the product of the cell density and the oxygen concentration. Michaelis Menten kinetics was not used for the oxygen consumption because the low concentration of oxygen in the scaffold would be much less than K_m, the Michaelis Menten constant.

The rate of cell growth was proportional to the concentration of oxygen in this model. Because the equilibration of oxygen occurred on a time scale much shorter than that for the cell growth, the transport of oxygen was quasi-steady such that the profile of oxygen concentration only changed when the cell density changed. The analysis showed the interior of the scaffold to be hypoxic due to the consumption of oxygen by cells located at the fluid-scaffold interface. Hypoxic cells have been experimentally confirmed in the interior of the scaffold (data

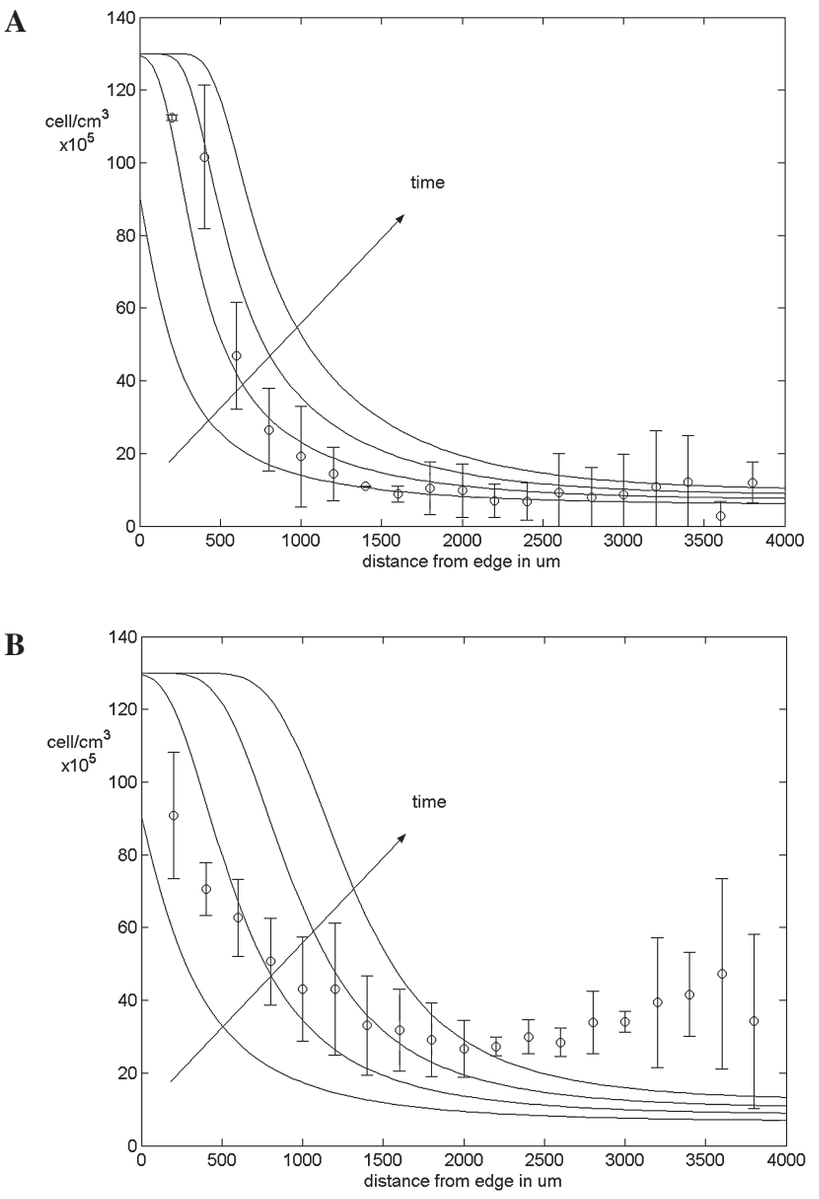

FIG. 8. Effect of varying the characteristic time on simulated cell density for the third scaffold in construct A with $L = 167$ μm. The simulated cell density for the middle portion **(A)** and the top and bottom portions **(B)** on day 5, 10, 20, and 40.

not shown). The gradient of oxygen resulted from the diffusion-reaction processes in the three-dimensional scaffold led to the formation of the gradient of cell density. As the cell population grew with time, the cell density along the edges of the scaffold increased the most, and a steeper gradient of oxygen concentration formed with time, which further limited the growth of cells in the interior of the scaffold.

In addition to the concentration of oxygen, the rate of cell growth also depended on the cell density in the simulation. A simple model was chosen where the growth rate was proportional to the cell density and to a logistic law that incorporated a maximal cell density beyond which the growth ceased. In the simulation, the growth rate initially increased with the cell density until it reached half of the maximum and subsequently decreased to zero at the maximal cell density. The maximal cell density was experimentally determined as the highest measured cell density. In this system, it was 1.3×10^7 cells/mL, but this number will likely be different for other cell-scaffold systems. This number is also significantly less than cell density in tissues, which ranges from 10^8 to 10^9 cells/mL.

The oxygen diffusivity was taken to be the typical value used for free diffusion in water. The scaffold ini-

tially was highly porous so the diffusion would be similar to that in water. As the cells grow to fill the pores, diffusion will become more restricted within the filled pores, as the diffusion in tissues is less than that in water. A dependence of diffusion on cell density would result in steeper gradient of the oxygen concentration in the simulation.

In all regions of the scaffold, the measured cell density was higher than the initial seeding density, indicating cell growth. Nevertheless, cell death could have occurred and was not accounted for in this model. Cell death can be documented by the release of cellular enzymes or by the activation of apoptosis. If necrosis or apoptosis was significant in the hypoxic region, then one might expect the measured cell density near the center of the scaffold to be lower than that predicted by the current simulation. This was not the case, particularly for the alternately seeded construct A, where the measured cell density near the scaffold layer-scaffold layer interface was much larger than the simulation.

The discrepancy between the model and experiment for the alternately seeded construct A may be due to another biophysical process. One possible explanation for the higher than predicted cell density is the physical discontinuity where successive scaffold layers meet. It is possible that transient convective flow may enter this discontinuity during culture medium changes. An alternative explanation for the observed gradient of cell density is cell migration within the scaffold, which is not considered by the current model. One may hypothesize that hypoxic cells in the interior of the scaffold migrate toward the higher oxygen concentration at the scaffold layer–scaffold layer interface, thereby creating the higher cell density near the edge. Targeted experiments are currently underway to test these hypotheses and to incorporate these biophysical processes in these models.

The mathematical model indicates that significant diffusion-reaction limitation occurs in cells growing in three-dimensional scaffolds. The cellular consumption of oxygen and nutrients near the bulk fluid-scaffold interface leads to less oxygen and nutrients in the inner core of the scaffold. This is likely the reason for the low cell density observed in the inner core. These considerations will be important in the design of scaffolds that can utilize this model to minimize diffusion-reaction constraints.

ACKNOWLEDGMENTS

This work was supported by grants from the Fubon Foundation (J.D.), the American Surgical Association Foundation (J.D.), the UCLA Academic Border Crossing Program (J.D., B.W.) and the National Science Foundation (V.C., J.K., J.L.).

REFERENCES

1. Nishimura, I., Garrell, R.L., Hedrick, M., Iida, K., Osher, S., and Wu, B. Precursor tissue analogs as a tissue-engineering strategy. Tissue Eng. **9,** S77, 2003.
2. Greenberg, S., Margulis, A., and Garlick, J.A. In vivo transplantation of engineered human skin. Meth. Mol. Biol. **289,** 425, 2004.
3. Sodian, R., Hoerstrup, S.P., Sperling, J.S., Daebritz, S.H., Martin, D.P., Schoen, F.J., Vacanti, JP., and Mayer, J.E., Jr. Tissue engineering of heart valves: in vitro experiences. Ann. Thorac. Surg. **70,** 140, 2000.
4. Burg, K.J., Holder, W.D., Jr., Culberson, C.R., Beiler, R.J., Greene, K.G., Loebsack, A.B., Roland, W.D., Eiselt, P., Mooney, D.J., and Halberstadt, C.R. Comparative study of seeding methods for three-dimensional polymeric scaffolds. J. Biomed. Mater. Res. **51,** 642, 2000.
5. Yang, T.H., Miyoshi, H., and Ohshima, N. Novel cell immobilization method utilizing centrifugal force to achieve high-density hepatocyte culture in porous scaffold. J. Biomed. Mater. Res. **55,** 379, 2001.
6. Carrier, R.L., Rupnick, M., Langer, R., Schoen, F.J., Freed, L.E., and Vunjak-Novakovic, G. Effects of oxygen on engineered cardiac muscle. Biotechnol. Bioeng. **78,** 617, 2002.
7. Freed, L.E., Langer, R., Marquis, J.C., and Vunjak-Novakovic, G. Kinetics of chondrocyte growth in cell-polymer implants. Biotechnol. Bioeng. **43,** 597, 1994.
8. Lee, M., Dunn, J.C.Y., and Wu, B.M. Scaffold fabrication by indirect three-dimensional printing. Biomaterials **26,** 4281, 2005.
9. Korecky, B., Hai, C.M., and Rakusan, K. Functional capillary density in normal and transplanted rat hearts. Can. J. Physiol. Pharmacol. **60,** 23, 1982.
10. West, C.M., Cooper, R.A., Loncaster, J.A., Wilks, D.P., and Bromley, M. Tumor vascularity: a histological measure of angiogenesis and hypoxia. Cancer Res. **61,** 2907, 2001.
11. Carrier, R.L., Rupnick, M., Langer, R., Schoen, F.J., Freed, L.E., and Vunjak-Novakovic, G. Perfusion improves tissue architecture of engineered cardiac muscle. Tissue Eng. **8,** 175, 2002.
12. Obradovic, B., Carrier, R.L., Vunjak-Novakovic, G., and Freed, L.E. Gas exchange is essential for bioreactor cultivation of tissue engineered cartilage. Biotechnol. Bioeng. **20,** 197, 1999.
13. Vunjak-Novakovic, G., Obradovic, B., Martin, I., and Freed, L.E. Bioreactor studies of native and tissue engineered cartilage. Biorheology **39,** 259, 2002.
14. Vunjak-Novakovic, G., Obradovic, B., Martin, I., Bursac, P.M., Langer, R., and Freed, L.E. Dynamic cell seeding of polymer scaffolds for cartilage tissue engineering. Biotechnol. Prog. **14,** 193, 1998.
15. Burg, K.J., Holder, W.D., Jr., Culberson, C.R., Beiler, R.J., Greene, K.G., Loebsack, A.B., Roland, W.D., Eiselt, P., Mooney, D.J., and Halberstadt, C.R. Comparative study of seeding methods for three-dimensional polymeric scaffolds. J. Biomed. Mater. Res. **51,** 642, 2000.
16. Whang, K., Tsai, D.C., Nam, E.K., Aitken, M., Sprague, S.M., Patel, P.K., and Healy, K.E. Ectopic bone formation

via rhBMP-2 delivery from porous bioabsorbable polymer scaffolds. J. Biomed. Mater. Res. **42,** 491, 1998.
17. Galban, C.J., and Locke, B.R. Effects of spatial variation of cells and nutrient and product concentrations coupled with product inhibition on cell growth in a polymer scaffold. Biotechnol. Bioeng. **64,** 633, 1999.
18. Galban, C.J., and Locke, B.R. Analysis of cell growth kinetics and substrate diffusion in a polymer scaffold. Biotechnol. Bioeng. **65,** 121, 1999.
19. Brown, D.A., Chou, Y.F., Beygui, R.E., Dunn, J.C., and Wu, B.M. Gelatin-embedded cell-polymer constructs for histological cryosectioning. J. Biomed. Mater. Res. **72,** 79, 2005.
20. Kim, J.S., Kang, K., and Lowengrub, J. Conservative multigrid methods for Cahn-Hilliard fluids. J. Comp. Phys. **193,** 511, 2004.
21. Trottenberg U., Oosterlee C., and Schuller A. Multigrid. San Diego: Academic Press, 2001.

Address reprint requests to:
James C.Y. Dunn, M.D., Ph.D.
MC 709818
10833 Le Conte Avenue
Los Angeles, CA 90095

E-mail: jdunn@mednet.ucla.edu